RSC Advances

PAPER

View Article Online
View Journal | View Issue

Cite this: *RSC Adv.*, 2020, **10**, 29378

TiO_2 nanoflowers based humidity sensor and cytotoxic activity

Pratik V. Shinde, [a] Snehal Gagare, [b] Chandra Sekhar Rout [a] and Dattatray J. Late *[b]

Received 6th June 2020
Accepted 27th July 2020

DOI: 10.1039/d0ra05007e

rsc.li/rsc-advances

We have systematically investigated the humidity sensing performance and cytotoxic activity of TiO_2 nanoflowers synthesized by hydrothermal method. Our result reveals that TiO_2 nanoflower based sensor devices show good performance at room temperature with a maximum sensitivity of ~815% along with a response time of ~143 s and a recovery time of ~33 s. Our findings also evaluate the cytotoxic effect of TiO_2 nanoflowers on human HepG2 cell lines. The cells are cultured in DMEM medium with varying concentrations of TiO_2 nanoflowers for 24, 48 and 72 hours respectively. The results indicate that TiO_2 nanoflower doses time dependently suppress the proliferation of HepG2 cell lines.

1. Introduction

There is a high demand for the development of inexpensive and reliable humidity sensor devices for control in various applications such as automation services, food processing, biomedical, pharmaceutical, metrology, nano-electronics, agriculture and structural health monitoring with high performance and good cyclic stability. The development of humidity sensor devices which can operate at room temperature is a real challenge and in high demand. Sensors based on oxide nanomaterials such as ZnO, SnO_2, Fe_2O_3, V_2O_5 are widely studied and commercially available in the market but they can only be operated at high temperature[1–6] raising safety issues. This has limited their widespread applications for monitoring, detection and precision operation in various industries for example electronic gadgets for healthcare, transportation, geo informatics *etc.*, humidity sensors devices have become increasingly important.

Owing to its importance for technological applications the anatase titanium dioxide (TiO_2) nanostructure has been widely investigated.[6–13] TiO_2 is known to be inexpensive, highly photoconductive and easily synthesized at low temperature using various physical and chemical methods. It is noteworthy that the TiO_2 is highly photostable material with high chemical stability, high refractive index ~ 2.7, high dielectric constant along with hardness and has wide bandgap of 3 eV.[14–19] The TiO_2 nanostructures have been widely used in a variety of industrial applications such as production of paper, plastics, cosmetics, paints, medicine, additives in food colorants and nutritional products.[20] Earlier studies reveals that metal oxide nanomaterials based sensor devices were not much suited for detection of high precision gas concentrations but are only able to detect the presence of targeted gases and give a counsel. The various morphology of TiO_2 nanostructure have reported as sensor for example alcohol,[21] NH_3,[22] NO_2 (ref. 23 and 24) and H_2 (ref. 25 and 26) *etc.* Further the humidity sensing applications of TiO_2 nanostructures were only reported for composite with other nanostructured materials.[27–30]

The TiO_2 nanoparticles has photocatalytic properties which are explored for its use as a disinfectant, antibiotic, biological sensor, tumor cell-killing agent, and gene targeting device.[31] The liver cancer in men is the fifth common cancer worldwide. Although chemotherapy and transplantation are widely acceptable clinical operations, the mortality of HCC still remains high attributed due to recurrence and drug-resistance.[32] This study highlights the influence of the TiO_2 nanoflower on HepG2 cell line growth inhibition, at various concentrations and for various treatment periods *in vitro*. The HepG2 cell line was selected as cell line has been widely used as the human liver cancer model cell line in the development of new anti-tumor medicines.[33–35] The earlier studies showed that TiO_2 nanoparticles with dose of ~5 g per kg body weight did not cause toxic effects in rats.[36,37] Fabian *et al.*[37] confirmed that rats exposed to TiO_2 nanoflower dose by a route can allows instantaneous systemic availability showed a predictable tissue Fabian distribution but no noticeable toxic effects, not much immune response, and no effect on organ function. Therefore, it was suggested that TiO_2 nanoparticles can be used safely in low amount of doses. In this paper we report facile synthesis of TiO_2 nanoflower like morphology and report its humidity sensing and cytotoxic activity.

2. Experimental methods

2.1 Synthesis of TiO_2 nanoflower like morphology

Hydrothermal method is widely used for the synthesis of various nanostructures due to low cost, fast reaction time, well

[a]Centre for Nano and Material Sciences, Jain Global Campus, Jakkasandra, Ramanagaram, Bangalore, 562112, Karnataka, India

[b]Centre for Nanoscience and Nanotechnology, Amity University Maharashtra, Mumbai-Pune Expressway, Bhatan 410206, India. E-mail: datta099@gmail.com; djlate@mum.amity.edu

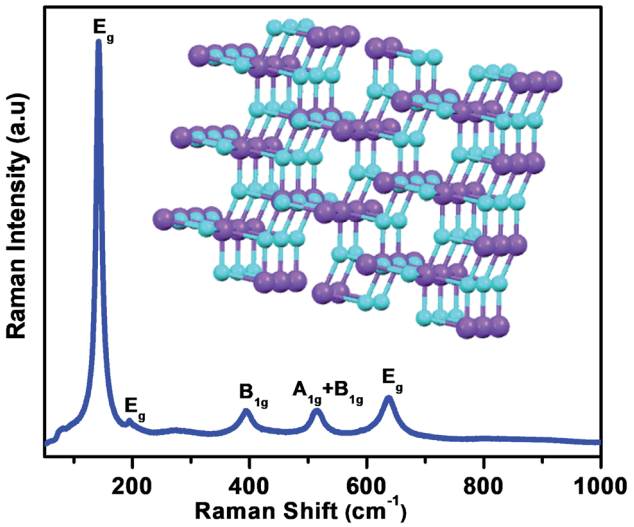

Fig. 1 Raman spectra of TiO_2 nanoflowers. Inset: Anatase structure of TiO_2.

controlled morphology and highly pure product. We have modified the original protocol of synthesis of TiO_2 nanostructures.[38,39] In brief the synthesis, 0.5 g of TiO_2 is mixed with 60 ml sodium hydroxide (10 M) and stirred vigorously.

The resultant solution was then added into Teflon lined stainless steel autoclave. The autoclave was sealed and placed in an oven at 150 °C for 72 h followed by natural cooling to room temperature. The reaction product was removed from the autoclave and rinsed thoroughly using 1 M dilute HCl. The product was further dried in a vacuum oven at 80 °C for 6 h. The final product of TiO_2 powder was further annealed for 15 h at 450 °C. All the chemicals used in this study were analytical grade (purity > 99%). The chemicals TiO_2 powder, sodium hydroxide pellets and the hydrochloric acid (32%) were purchased from the S D fine-chem Limited, Bangluru, India.

2.2 Structural and morphological characterizations

The as synthesized TiO_2 powder obtained were characterized with scanning electron microscopy (SEM), transmission electron microscopy (TEM) and Raman spectroscopy. The TEM analyses were done using the instrument FEI TECNAI G2 F-20 (FEG), Raman spectroscopy was done with Horiba JY Lab Raman HR 800 Micro Raman Spectrometer equipped with a 632.8 nm laser. For TEM characterization samples were prepared by first dispersing the powder sample in ethanol and then drop casting of the powder TiO_2 nanoflower over a copper TEM grid coated with carbon film. For Raman characterization the samples were drop casted directly onto the silicon substrate.

2.3 Humidity sensor device fabrication

The sensor devices were fabricated in two probe geometry by drop casting the TiO_2 nanoflower powder sample onto ITO patterned electrode with separation of ~250 μm. The as synthesized TiO_2 nano powder sample were dispersed in ethanol solvent for drop casting purpose, followed by annealing of the device in vacuum oven at 80 °C.

2.4 Humidity test

The aqueous saturated salt solutions of LiCl, $MgCl_2$, K_2CO_3, NaBr, KI, NaCl, KCl and K_2SO_4 were used to generate different relative humidity (RH) environments. It is known that aqueous saturated solutions of these salt solutions generate approximate

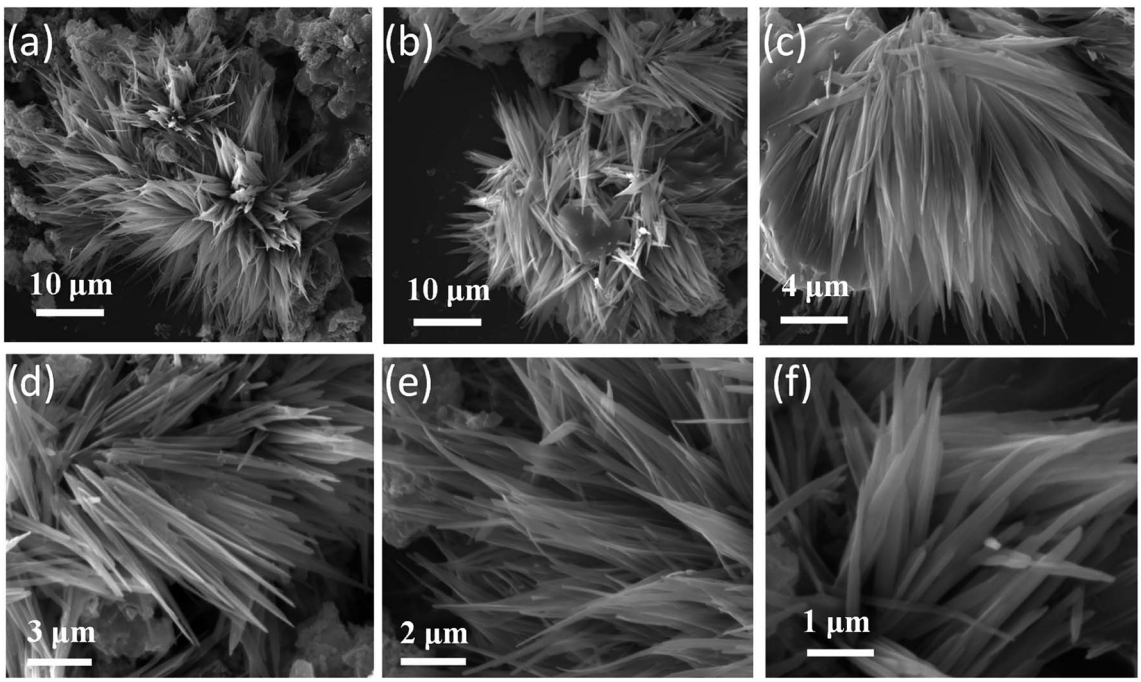

Fig. 2 (a–f) SEM images of TiO_2 nanoflower synthesized using simple hydrothermal method.

relative humidities of 11.3%, 32.8%, 43.16%, 57.57%, 68.86%, 75.29%, 85.06% and 97.3% respectively.[40–47] The current–voltage (*I–V*) measurements were carried out using the dual channel Keithley 2612A Source meter.

2.5 Cytotoxicity assay

2.5.1 Cell line and culture conditions. HepG2 cell cultures were received from National Centre for Cell Sciences (NCCS), Pune, India. Stock cells were cultured in Dulbecco's modified Eagle's medium (DMEM). The medium was supplemented with 10% inactivated Fetal Bovine Serum (FBS), penicillin (100 IU ml^{-1}) and amphotericin B (streptomycin (100 g ml^{-1})) in an humidified atmosphere of 5% CO_2 until confluent. The cells were dissociated with TPVG solution [0.2% trypsin, 0.02% ethylene diamine tetraacetic acid (EDTA), 0.05% glucose in phosphate buffered saline (PBS)]. The stock cultures were grown in 25 cm^2 culture flasks and all experiments were carried out in 96 microtitre plates (Tarsons India Pvt. Ltd., Kolkata, India). The cell viability were tested by 3-(4,5-dimethyl thiazol-2-yl)-2, 5-diphenyltetrazolium bromide (MTT) Assay. The colorimetric assay is based on the capacity of mitochondria succinate dehydrogenase enzymes in living cells to reduce the yellow water-soluble substrate (MTT) into an insoluble purple coloured formazan product which is measured spectrophotometrically. Since the reduction of MTT can only occur in metabolically active cells, the level of activity is a measure of the cells.[48] The monolayer cell culture was trypsinized and the cell count was adjusted to 1.0×10^5 cells per ml using a medium containing 10% FBS and were used for the determination of cell viability by MTT assays as described by Francis and Rita.[48] The absorbance was measured using a microplate reader at a wavelength of 540 nm. The percentage of cell viability that is amount of cell surviving after treatment with TiO_2 nanoflower were then analyzed by the following equation:

$$\% \text{ cellular viability} = \text{Abs cells} + \text{Nps} - \text{AbsNps/Abs cells} - \text{Abs DMEM} \times 100 \quad (1)$$

The % inhibition is calculated as:

$$\% \text{ inhibition} = 100 - \% \text{ cell viability} \quad (2)$$

2.5.2 Statistical analysis. The data was analyzed statistically using one way ANOVA replication ($P \leq 0.05$) to assess the statistical significance of difference.

3. Results and discussion

The Raman spectroscopy investigations were carried out to examine the crystal phase of anatase TiO_2 nanoflower. It is

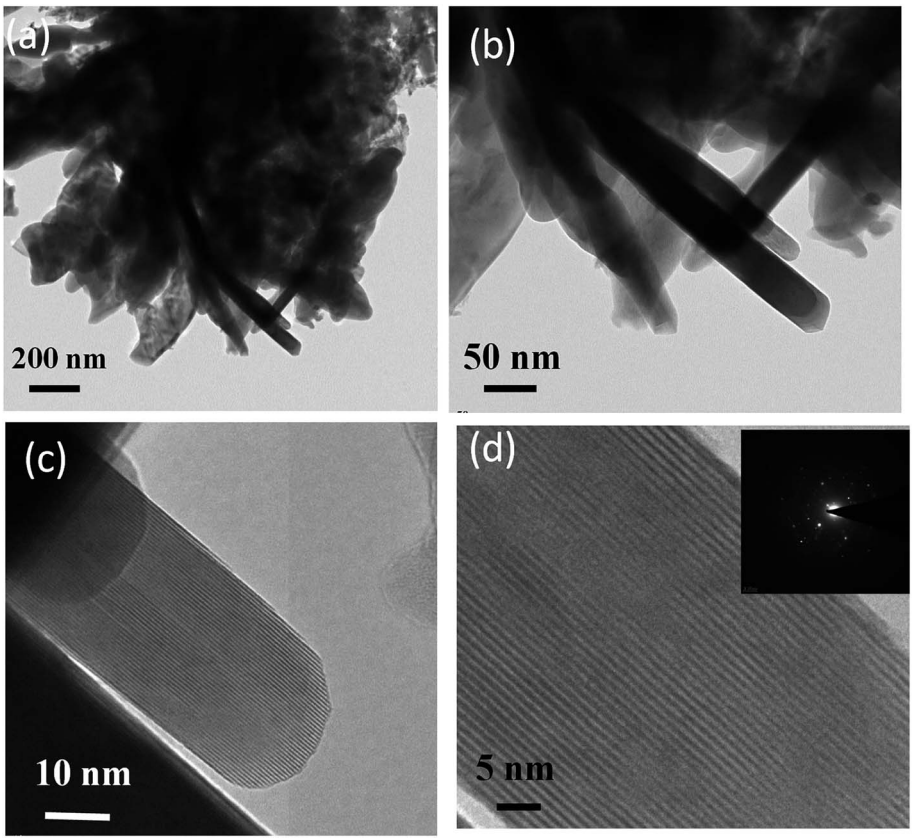

Fig. 3 TEM analysis of as synthesized TiO_2 nanoflowers, (a and b) low resolution TEM images, (c and d) high resolution TEM images. Inset of (d) shows typical SAED pattern indicating highly crystalline nature of as synthesized TiO_2 nanoflower.

known that the bulk anatase TiO_2 has a tetragonal structure (space group $I4_1/amd$) which contains the twelve atoms per unit cell with lattice parameters $a = 3.784$ Å and $c = 9.514$ Å. As per the factor group analysis, anatase phase has six Raman active modes ($A_{1g} + 2B_{1g} + 3E_g$). The Raman spectrum of anatase single crystal has six modes which appears ~144 cm^{-1} (E_g), 197 cm^{-1} (E_g), 399 cm^{-1} (B_{1g}), 513 cm^{-1} (A_{1g}), 519 cm^{-1} (B_{1g}), and 639 cm^{-1} (E_g).[49] Fig. 1 shows the typical Raman spectra of TiO_2 nanoflower recorded at room temperature. The Raman peaks at around 143, 395, 515 and 637 cm^{-1} are assigned to bulk anatase TiO_2. Inset of Fig. 1 shows the anatase crystal structure of TiO_2.

Fig. 2 shows the typical SEM images of as synthesize TiO_2 nanoflower like morphology. The morphology also reflects the mesoporous like structure of TiO_2. The TiO_2 nanoflower with petal length 20–15 μm were clearly seen in the SEM image. The nanopetals of TiO_2 are found to be bind in bundles. It has been observed that, the typical TiO_2 flower consisting large number of uniform petals with lateral dimension in micron size and thickness ~ 10 nm as confirmed from the TEM analysis. The Fig. 3(a and b) shows typical low resolution TEM images of TiO_2 nanoflower. Fig. 2(c and d) shows typical high resolution TEM images of TiO_2 nanoflower petals. The high resolution TEM image also reflects the good crystalline quality of as synthesized TiO_2 nanoflower sample. Fig. 3(d) inset shows the selected area electron diffraction pattern of TiO_2 nanoflower, which also indicates the good quality of the as prepared TiO_2 nanoflower sample.

The current–voltage (I–V) characteristics of TiO_2 nanoflower based humidity sensor were carried out at various relative humidities. Fig. 4(a) shows the typical I–V characteristics of TiO_2 nanoflower based humidity sensor device at various relative humidities. From the I–V characteristics, it is seen that the current increases as function of increase in the relative humidity. The sensitivity were calculated by using following equation,

$$S = \frac{R_{97} - R_{11}}{R_{97}} \times 100\ \% \quad (3)$$

where, S is the sensitivity, R_{97} is resistance at 97.3% relative humidity and R_{11} is the resistance in 11.3% relative humidity. Fig. 4(b) shows the typical sensitivity/resistance of the sensor device as function of relative humidity. The maximum sensitivity of ~815% was observed for TiO_2 nanoflower based humidity sensor. Fig. 4(c) shows the typical current–time (I–t) cycles of humidity sensor device based on TiO_2 nanoflowers. For recording I–t cycle, the device were first kept in 11% relative

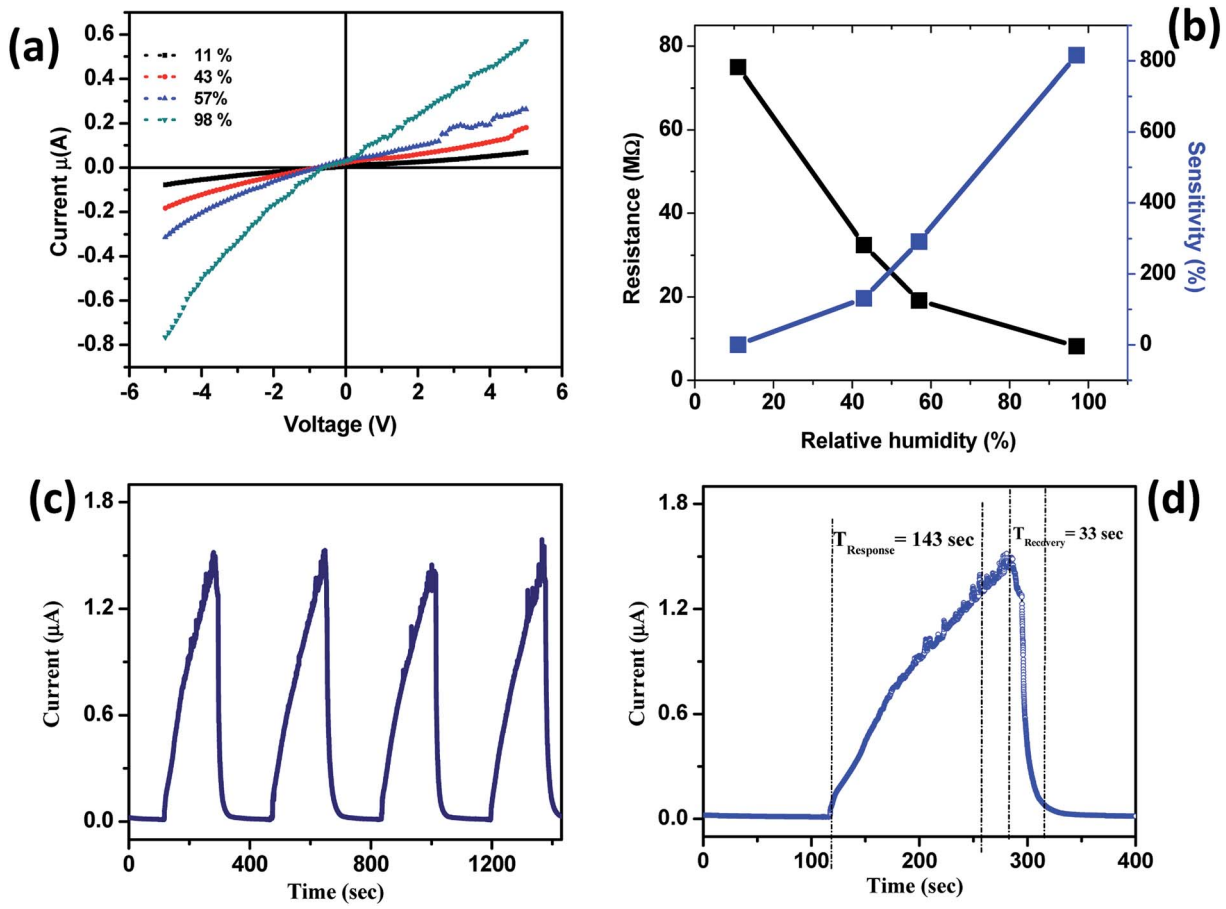

Fig. 4 Humidity sensing performance of TiO_2 based humidity sensor device. (a) Typical I–V characteristics of TiO_2 nanoflower based humidity sensor at various relative humidities, (b) typical sensitivity/resistance of sensor device as function of relative humidity, (c) typical I–t cycles of sensor device showing high stability of the device and (d) typical single I–t cycle of the sensor device showing response and recovery time.

humidity and then subsequently transferred to 97% relative humidity. Fig. 4(d) shows the typical one such *I–t* cycle of the humidity sensor device which used to calculate the typical response time ~ 143 s and recovery time of ~33 s. Our result indicates that sensor has very good recovery time at room temperature. Our results open up several avenues to fabricate the TiO_2 nanoflower based humidity sensor devices to operate at room temperature. The typical gas sensor mechanism involves injection of water molecules into the sensor chamber, after adsorbed onto the semiconductor surface the charges transfer which results into the change in the resistance of the sensor device.[50] In reality, the change in the resistance consequence from the fact of charge transfer and Schottky barrier.[51–53] The adsorption and desorption of gas molecules leads to the shifting of Fermi level toward the conduction band or valence band.[50]

Fig. 5 shows the typical optical images of TiO_2 cytotoxic activity after (a) 24 h, (b) 48 h and (c) 72 h. The HepG2 cell line was treated with various concentrations of TiO_2 nanoparticles ranging from 10 to 100 μg ml^{-1}, and the cell growth inhibition was measured by the MTT assay. The Fig. 6(a) shows the effect of different concentration of TiO_2 nanoflowers against HepG2 cell lines at 24, 48, 72 hours respectively. The results showed that the cell growth inhibition was induced in a time-dependent manner after 24, 48 and 72 h exposure of human HepG2 cell line to TiO_2 nanoflower using the MTT assay, and as the concentration of TiO_2 were increased from 10 to 100 μg ml^{-1}, the cell viability decreased, in a dose-dependent manner. After 24 h, the various concentrations of TiO_2 nanoparticles had not significant suppression on the proliferation of HepG2 cell line. The cell growth inhibition of HepG2 cell line significantly increased after 48 h exposure to TiO_2 concentrations of 40, 70 and 100 μg with 15%, 25% and 30% respectively.

Fig. 6(b) shows the effect of different incubation times of TiO_2 nanoflowers against HepG2 cell lines (the experiment is repeated three times independently with values indicating the mean). Fig. 6(b) clearly indicates decreasing in the cell viability as the exposure time to TiO_2 nanoflowers is increased. The results showed that cell growth inhibition was induced in a time-dependent manner after 24, 48 and 72 h exposure of human HepG2 cell line. The cytotoxicity assay were then carried out using the MTT with different concentration of TiO_2 as increased from 10 to 100 μg ml^{-1}, the cell viability were found to be decreased, in a dose-dependent manner. The highest cytotoxicity of this solution against HepG2 was 34% of cell growth inhibition by 100 μg ml^{-1} after 72 h. For all statistical analysis the one way anova was used to find statistical difference between measurements of control and treatment. The results of cytotoxic activity conducted in the above study are similar with the studies of P. Govindhan *et al.* also highlights, that TiO_2@-SiO_2–Ag was effective against HepG2 and Caco-2 cancer cell line, as it led to inhibition in cell growth.[54] The typical mechanism

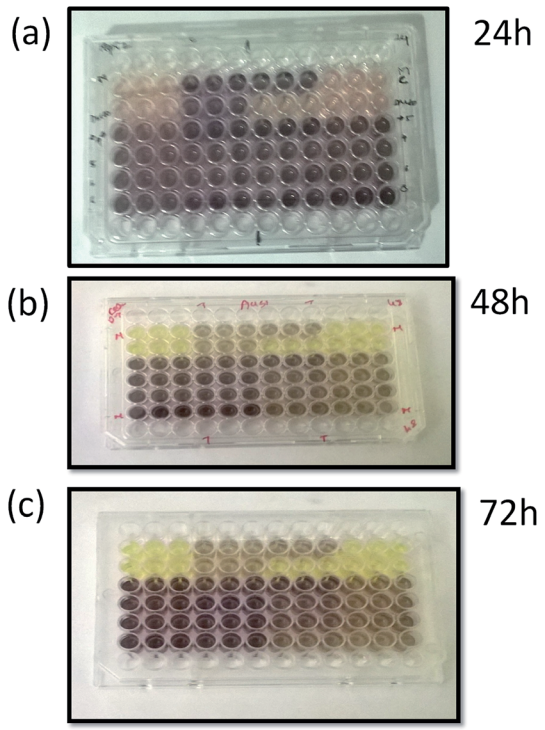

Fig. 5 Optical images of TiO_2-anti-cancer activity after (a) 24 h, (b) 48 h and (c) 72 h.

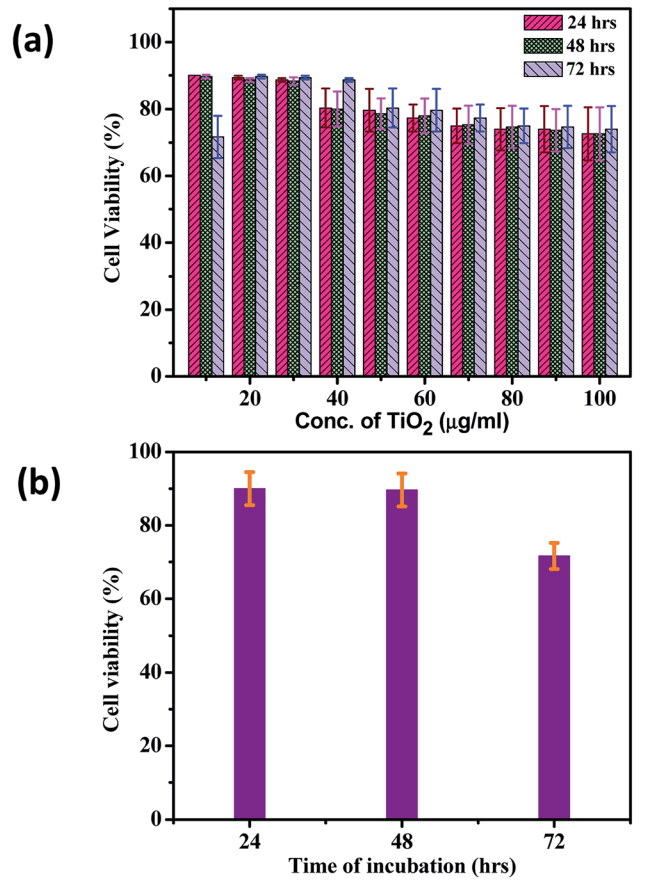

Fig. 6 (a) Effect of different concentration of TiO_2 nanoflowers against HepG2 cell lines at 24, 48, 72 hours respectively. (b) Effect of different incubation times of TiO_2 nanoflowers against HepG2 cell lines (the experiment is repeated three times independently with values indicating the mean).

involves the metabolism of TiO_2 nanoflowers induced oxidative stress and which results into the toxicity. The TiO_2 nanoflower induce the formation of reactive oxygen species which increases the oxidative stress, this further causes the redox imbalance in the cell.[55,56] The reactive oxygen species (ROS) induction by TiO_2 nanostructures is basically because of pro-oxidant functional groups on their reactive surface or due to the TiO_2 and cell interactions formation which causes the oxidative stress.[57,58] There is a cellular mechanism which protects the cell from oxidative stress, like the enzymatic and non-enzymatic. But if the cell is unable to overcome the oxidative stress it results in the damage to the biomolecules like DNA, Protein and lipid which leads to apoptosis resulting in the cell demise.[59–62]

4. Conclusions

In conclusion, we have reported the synthesis of TiO_2 nanoflowers with a length of petal 15–20 μm and thickness ~ 10 nm. The humidity sensor based on TiO_2 nanoflower were fabricated which shows high sensitivity of ~815% and fastest recovery time of ~33 s. The work also represents a new observation on cytotoxic effect of TiO_2 nanoflowers on HepG2 (human liver cancer cell line) cell demise. TiO_2 nanoflowers might provide a controlled and targeted way to deliver the encapsulated anticancer drugs and thus result in high efficacy with low side effects. The results also suggest that TiO_2 may provide a degree of toxicity based on the interactions between the time and its concentrations. However, more studies were needed to elucidate the effects of TiO_2 and to clarify the mechanisms of the TiO_2 toxicity on cells with the aim of developing new strategies for the treatment of cancer and other illness. This work provided a new way to develop economic and well-designed TiO_2 nanostructured morphology for multifunctional applications.

Author contributions

DJL conceived the idea, designed experiments, and analyzed the experimental data and co-wrote the manuscript. PVS performed the synthesis, characterization and humidity sensing measurements of the TiO_2 nanopowder sample. SG performed the cytotoxic effect of TiO_2 nanoflowers. All authors were involved in discussion and have read the manuscript and agree to its contents.

Conflicts of interest

All authors declare that they do not have any conflicts of interest.

Acknowledgements

Authors thank Director, CSIR-National Chemical Laboratory Pune (India) and Director, National Centre for Cell Sciences (NCCS), Pune (India) for the support. Authors thank Prof. D. S. Rao Vice-chancellor, Amity University Mumbai for support and encouragement. CSR acknowledges Department of Science and Technology (DST)-SERB Early Career Research project (Grant No. ECR/2017/001850), DST-Nanomission (DST/NM/NT/2019/205(G)), Karnataka Science and Technology Promotion Society (KSTePS/VGST-RGS-F/2018-19/GRD NO. 829/315).

Notes and references

1 M. Prudenziati and B. Morten, *Sens. Actuators*, 1986, **10**, 65–82.
2 S. K. Joshi, C. N. R. Rao, T. Tsuruto and S. Nagakura, *Gas sensor Materials in 'New Material'*, Narosa Publishing House, New Delhi, India, 1992.
3 B. M. Kulwicki, *J. Am. Ceram. Soc.*, 1991, **74**, 697–708.
4 N. Yamazoeand and Y. Shimizu, *Sens. Actuators*, 1986, **10**, 379–398.
5 M. J. Madou and S. R. Morrison, *Chemical sensing with solid-state devices*, Academic Press Inc., San Diego, CA, 1989.
6 A. M. Azad, S. A. Akbar, S. G. Mhaisalkar, L. D. Birkefeld and K. S. Goto, *J. Electrochem. Soc.*, 1992, **139**, 3690–3704.
7 X. Yang, Z. Li, G. Liu, J. Xing, C. Sun, H. G.Yang and C. Li, *CrystEngComm*, 2011, **13**, 1378–1383.
8 A. Fujishima and K. Honda, *Nature*, 1972, **238**, 37–38.
9 M. Grätzel, *Nature*, 2001, **414**, 338–344.
10 X. Chen and S. S. Mao, *Chem. Rev.*, 2007, **107**, 2891–2959.
11 C. Dinh, T. Nguyen, F. Kleitz and T. Do, *ACS Nano*, 2009, **3**, 3737–3743.
12 C. Liu, H. Sun and S. Yang, *Chem.–Eur. J.*, 2010, **16**, 4381–4393.
13 H. G. Yang and H. C. Zeng, *J. Phys. Chem. B*, 2004, **108**, 3492–3495.
14 J. H. Kim, D. H. Kimand and T. Y. Seong, *Ceram. Int.*, 2015, **41**, 3064–3068.
15 C. Dette, M. A. Pérez-Osorio, C. S. Kley, P. Punke, C. E. Patrick, P. Jacobson, F. Giustino, S. J. Jung and K. Kern, *Nano Lett.*, 2014, **14**, 6533–6538.
16 K. Kaviyarasu, N. Geetha, K. Kanimozhi, C. M. Magdalane, S. Sivaranjani, A. Ayeshamariam, J. Kennedy and M. Maaza, *Mater. Sci. Eng., C*, 2017, **74**, 325–333.
17 W. Fan, X. Yu, H. C. Lu, H. Bai, C. Zhang and W. Shi, Fabrication of TiO_2/RGO/Cu_2O heterostructure for photoelectrochemical hydrogen production, *Appl. Catal., B*, 2016, **181**, 7–15.
18 T. Georgakopoulos, M. V. Sofianou, K. Pomoni, N. Todorova, T. Giannakopoulou and C. Trapalis, *Mater. Sci. Semicond. Process.*, 2016, **56**, 386–393.
19 D. S. Kim and S. Y. Kwak, *Appl. Catal., A*, 2007, **323**, 110–118.
20 N. Rihane, B. Younes, S. Amara, I. Mrad, I. Ben-Slama, M. Jeljeli, K. Omri, J. El Ghoul, L. El Mir, K. Ben Rhouma, H. Abdelmelek and M. Sakly, *Environ. Sci. Pollut. Res.*, 2015, **22**, 8728–8737.
21 Y. Wang, J. Liu, M. Wang, C. Pei, B. Liu, Y. Yuan, S. Liu and H. Yang, *Inorg. Chem.*, 2017, **56**, 1504–1510.
22 W. Meng, L. Dai, W. Meng, H. Zhou, Y. Li, Z. He and L. Wang, *Sens. Actuators, B*, 2017, **240**, 962–970.
23 T. Xie, N. Sullivan, K. Steffens, B. Wen, G. Liu, R. Debnath, A. Davydov, R. Gomez and A. Motayed, *J. Alloys Compd.*, 2015, **653**, 255–259.

24 S. Boyadjiev, V. Georgieva, L. Vergov, Z. Baji, F. Gáber and I. M Szilágyi, *J. Phys.: Conf. Ser.*, 2014, **559**, 012013.
25 J. Bai and B. Zhou, *Chem. Rev.*, 2014, **114**, 10131–10176.
26 J. Lee, D. H. Kim, S.-H. Hong and J. Y. Jho, *Sens. Actuators, B*, 2011, **160**, 1494–1498.
27 C. H. Ashok and K. V. Rao, *Superlattices Microstruct.*, 2014, **76**, 46–54.
28 N. K. Pandey, K. Tiwari and A. Roy, *Bull. Mater. Sci.*, 2012, **35**, 347–352.
29 C. H. Ashok and K. V. Rao, *J. Mater. Sci.: Mater. Electron.*, 2016, **27**, 8816–8825.
30 D. N. Huyen, N. T. Tung, N. D. Thien and L. H. Thanh, *Sensors*, 2011, **11**, 1924–1931.
31 J. J. Wang, B. J. Sanderson and H. Wang, *Mutat. Res.*, 2007, **628**, 99–106.
32 P. Thevenot, J. Cho, D. Wavhal, R. B. Timmons and L. Tang, *Nanomedicine*, 2008, **4**, 226–236.
33 O. Dudeck and J. Ricke, *Expert Opin. Drug Delivery*, 2011, **8**, 1057–1069.
34 Y. Zhu, J. W. Eaton and C. Li, *PLoS One*, 2012, **7**, e50607.
35 T. Lozano, M. Rey, E. Rojas, S. Moya, J. Fleddermann, I. Estrela-Lopis, E. Donath, B. Wang, Z. Mao, C. Gao and Á. González-Fernández, *J. Phys.: Conf. Ser.*, 2011, **304**, 012046.
36 J. Wang, G. Zhou and C. Chen, *Toxicol. Lett.*, 2007, **168**, 176–185.
37 E. Fabian, R. Landsiedel and L. Ma-Hock, *Arch. Toxicol.*, 2008, **82**, 151–157.
38 G. Armstrong, A. R. Armstrong, J. Canales and P. G. Bruce, *Chem. Commun.*, 2005, 2454–2456.
39 Y. X. Zhang, G. H. Li, Y. X.Jin, Y. Zhang, J. Zhang and L. D. Zhang, *Chem. Phys. Lett.*, 2002, **365**, 300–304.
40 D. Bharatula, M. B. Erande, I. S. Mulla, C. S. Rout and D. J. Late, *RSC Adv.*, 2016, **6**, 105421–105427.
41 A. S. Pawbake, S. R. Jadkar and D. J. Late, *Mater. Res. Express*, 2016, **3**, 105038.
42 M. B. Erande and D. J. Late, *Adv. Device Mater.*, 2016, **2**, 8–14.
43 D. J. Late, *Microporous Mesoporous Mater.*, 2016, **225**, 494–503.
44 M. B. Erande, M. Pawar and D. J. Late, *ACS Appl. Mater. Interfaces*, 2016, **8**, 11548–11556.
45 L. Khandare, S. S. Terdale and D. J. Late, *Adv. Device Mater.*, 2016, **2**, 15–22.
46 P. K. Kannan, D. J. Late, H. Morgan and C. S. Rout, *Nanoscale*, 2015, **7**, 13293–13312.
47 D. J. Late, Y. K. Huang, B. Liu, J. Acharya, S. N. Shirodkar, J. Luo, A. Yan, D. Charles, U. V. Waghmare, V. P. Dravid and C. N. R. Rao, *ACS Nano*, 2013, **7**, 4879–4891.
48 D. Francis and L. Rita, *J. Immunol. Methods*, 1986, **89**, 271–277.
49 T. Ohsaka, *J. Phys. Soc. Jpn.*, 1980, **48**, 1661–1668.
50 H. Chen, Y. Chen, H. Zhang, D. W. Zhang, P. Zhou and J. Huang, *Adv. Funct. Mater.*, 2018, 1801035.
51 J. Nah, S. B. Kumar, H. Fang, Y.-Z. Chen, E. Plis, Y.-L. Chueh, S. Krishna, J. Guo and A. Javey, *J. Phys. Chem. C*, 2012, **116**, 9750.
52 X. Cui, M. Freitag, R. Martel, L. Brus and P. Avouris, *Nano Lett.*, 2003, **3**, 783.
53 E. L. Gui, L.-J. Li, K. Zhang, Y. Xu, X. Dong, X. Ho, P. S. Lee, J. Kasim, Z. Shen and J. A. Rogers, *J. Am. Chem. Soc.*, 2007, **129**, 14427.
54 P. Govindhan and C. Pragathiswaran, *J. Nanosci. Nanotechnol.*, 2016, **2**, 173–175.
55 W. Lin, I. Stayton, Y. W. Huang, X. D. Zhou and Y. Ma, *Toxicol. Environ. Chem.*, 2008, **90**, 983–996.
56 L. Weisheng, Y. Xu, C. C. Huang, Y. Ma, K. B. Shannon, D. Chen and Y. W. Huang, *J. Nanopart. Res.*, 2009, **11**(1), 25–39.
57 A. M. Knaapen, P. J. Borm, C. Albrecht and R. P. Schins, *Int. J. Cancer*, 2004, **109**, 799–809.
58 L. Risom, P. Møller and S. Loft, *Mutat. Res.*, 2005, **592**, 119–137.
59 S. G. Kang, A. L. Brown and J. H. Chung, *J. Biol. Chem.*, 2007, **282**, 6090–6097.
60 W. Lin, Y. W. Huang, X. D. Zhou and Y. Ma, *Toxicol. Appl. Pharmacol.*, 2006, **217**, 252–259.
61 W. Lin, Y. W. Huang, X. D. Zhou and Y. Ma, *Int. J. Toxicol.*, 2006, **25**, 451–457.
62 B. Fahmy and S. A. Cormier, *Toxicol. In Vitro*, 2009, **23**, 1365–1371.

